molecular pharmaceutics

pubs.acs.org/molecularpharmaceutics

Article

Knowledge-Based Design of 5-Fluororacil Prodrug Liposomal Formulation: Molecular Packing and Interaction Revealed by Interfacial Isotherms and X-ray Scattering Techniques

Tiep Pham, Paola Leon Plata, Pin Zhang, Anand Vellara, Wei Bu, Binhua Lin, Gang Cheng, and Ying Liu*

Cite This: *Mol. Pharmaceutics* 2021, 18, 4331−4340

Read Online

ACCESS | Metrics & More | Article Recommendations | Supporting Information

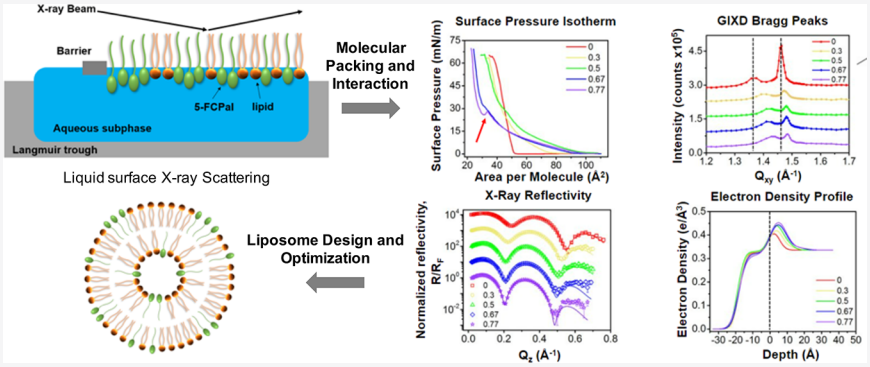

ABSTRACT: Prodrugs and nanoformulations are two effective strategies for sustained drug release and targeting drug delivery. In this study, we combined the two strategies to judiciously design the liposome formulation incorporating an amphiphilic prodrug of 5-fouroracil (5-FU), named 5-FCPal, for sustained drug release and enhanced bioavailability. 5-FCPal is an analogue of capecitabine (N^4-pentyloxycarbonyl-5′-deoxy-5-fluorocytidine, Xeloda) by substituting the pentyl group at the N^4 position with the palmityl. The amphiphilic molecule of 5-FCPal can self-assemble with the phospholipids to form stable vesicle structures with high drug loading. Although lipid vesicles have been widely studied and commercially used for clinical applications, because of the enormous options of the lipids and the equitable balance of hydrophobicity and bioavailability, it is essential to fundamentally understand the molecular interactions when designing and optimizing the liposomal prodrug formulations. We report the study of using X-ray liquid surface scattering techniques integrated with a Langmuir trough to explicitly reveal the interfacial behavior of the monolayer membrane of 5-FCPal with various saturated and unsaturated lipids with positively charged, neutral, and negatively charged head groups. More specifically, interfacial packing of the molecules was quantified using interfacial isotherms, X-ray reflectivity (XR), and grazing-incidence diffraction (GIXD). The results indicate that the interactions between the prodrug and the cationic lipids are most favorable. The highest drug loading is quantified by increasing the molar ratio of the prodrug until stable monolayer structures were disrupted by the multiple-layer domain of prodrug aggregates. Stable liposomes of 100 nm with 50% drug loading of 5-FCPal were generated based on the findings from the X-ray studies.

KEYWORDS: *amphiphilic prodrug, lipids, X-ray reflectivity, grazing incidence diffraction, liposomes, molecular packing and interaction*

INTRODUCTION

Prodrug and nanoformulations are two effective strategies to prolong drug release, reduce toxicity, and improve bioavailability. Prodrug modification is a chemical approach by either covalently attaching the hydrophilic drug (i.e., peptides) with an alkyl chain to increase drug lipophilicity for efficient passive membrane permeation[1,2] or conjugating the drug with a hydrophilic molecule for higher solubility and therefore higher bioavailability (i.e., PEGylation and albumin conjugation with hydrophobic drugs).[3,4] Nanoformulation is a physical approach to shift the pharmacokinetic properties of the drug by encapsulating or incorporating the therapeutic compounds with polymers or lipids to form nanostructures. Nanoparticles may promote passive targeting due to the enhanced permeation and retention (EPR) effect and offer additional advantages for active targeting by surface modification. Among

Received: June 20, 2021
Revised: October 24, 2021
Accepted: October 25, 2021
Published: November 5, 2021

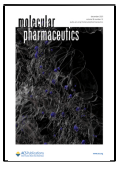

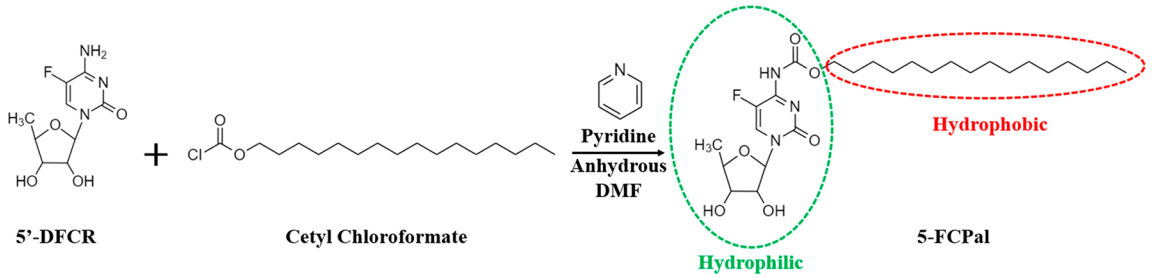

Figure 1. Synthesis of 5-FCPal.

different types of nanoformulations, liposomes, dispersed lipid nanovesicles with a liquid crystalline fluid lamellar phase, are the most widely used due to their similar compositions as the cell membranes. To date, several liposome-based formulations of cancer chemotherapies are commercially available, such as Doxil[5−7] and recently developed COVID-19 mRNA vaccines.[8,9]

5-Fluorouracil (5-FU) was rationally designed to treat solid malignant tumors, such as colorectal cancer and breast cancer.[10,11] However, 5-FU displays severe toxicities, quickly loses its efficacy due to poor distribution to tumor sites and extreme fast metabolism, and easily develops drug resistance.[12−14] Numerous derivatives and prodrugs have been designed and synthesized to improve the physicochemical and pharmacokinetic properties of 5-FU, among which capecitabine (Xeloda) has been approved by the Food and Drug Administration (FDA) as an oral drug for the treatment of colon, metastatic colorectal, and metastatic breast cancer. Capecitabine is converted to 5-FU through three metabolic steps, with the last step preferentially in targeted tumor tissues.[14,15] Although capecitabine significantly reduces 5-FU nonspecific cytotoxicity and increase drug bioavailability in the tumor, it still suffers from a very short half-life inside the human body and therefore frequent dosages and significant side effects. The design of effective, sustained-release systems with balanced physicochemical and pharmaceutic properties is still challenging. Recent studies by Drummond et al. demonstrated that, by increasing the size of the carbon chain conjugated to 5′-deoxy-5-Fluorocytidine (5′-DFCR), more hydrophobic prodrugs of 5-FU (an analogue of capecitabine) could possess longer metabolism time and better bioavailability.[16] The 5-FU prodrug with the longer carbon chain of palmityl significantly slows down the growth of mouse 4T1 breast tumor and halt the growth of human MDA-MB-231 breast tumor in mouse xenografts.[13,16] These prodrugs were tested in the crystal forms. The nanoformulations of capecitabine analogues were never investigated.

In this study, we report the synthesis of a capecitabine analogue by replacing the pentyl group with a longer alkyl chain (palmityl) at the N^4 position of 5′-deoxy-5-Fluorocytidine (5′-DFCR) through carbamate bonding, which ensures the same three-step enzymatic degradation pathways as capecitabine (Figure 1).[17] This prodrug is named as 5-FCPal, which is amphiphilic and may be incorporated into liposomes through hydrophobic interaction with the tail groups and electrostatic interaction with the head groups. Embedding the amphiphilic therapeutic molecules changes the packing and molecular interaction. On the other hand, the design of the liposomes directly decides the drug loading and stability, and therefore pharmacokinetics and efficacy. A wide range of choices of different lipid combinations allows the modification of liposome behavior in vivo and their design according to specific therapeutic needs. Nonetheless, the number of possibilities is enormous, and optimization of the structure is not feasible by empirical trials. Systematic understanding of molecular interactions is necessary but challenging to achieve.

Synchrotron X-ray reflectivity (XR) and grazing-incidence diffraction (GIXD) are powerful techniques to reveal the molecular interaction between the drug and lipid molecules, which provide the fundamental information for the judicious design of liposomal formulations embedding amphiphiles with high drug loading. We have previously employed XR and GIXD to reveal the spontaneous collapsing of the fatty acid after enzyme-catalyzed degradation of the phospholipid and evaluated the effects of polyethylene glycol (PEG) on enzyme adsorption and lipid degradation and reorganization.[18,19] By integrating a Langmuir trough with the synchrotron X-ray liquid surface scattering techniques, we systematically studied the monolayer packing of 5-FCPal and various lipids at the air−water interface. Five representative saturated and unsaturated lipids of different headgroup charges were employed in the study, including lipids with positively charged head groups (i.e., 1,2-stearoyl-3-trimethylammonium-propane (DSTAP) and 1,2-dioleoyl-3-trimethylammonium-propane (DOTAP)), neutral zwitterionic head groups (i.e., 1,2-dipalmitoyl-*sn*-glycero-3-phosphocholine (DPPC) and 1,2-dioleoyl-*sn*-glycero-3-phosphocholine (DOPC)), and negatively charged head groups (i.e., 1,2-dipalmitoyl-*sn*-glycero-3-phospho-(1′-rac-glycerol) (DPPG)).

EXPERIMENTAL SECTION

Materials and Reagents. DSTAP, DOPC, DPPC, DOPC, DPPG, 1,2-dipalmitoyl-*sn*-glycero-3-phosphoethanolamine-*N*-(lissamine thodamine B sulfonyl) (ammonium salt) (DPPE-Rhod, Ex/Em 560/583 nm), and 1,2-dipalmitoyl-*sn*-glycero-3-phosphoethanolamine-*N*-[methoxy(polyethylene glycol)-5000] (ammonium salt) (DPPE-PEG5k) were purchased from Avanti Polar Lipids. 5′-DFCR was purchased from Cayman Chemical, and hexadecyl chloroformate was purchased from TCI America. Ethyl acetate and hexane were purchased from BDH. Other organic solvents (including acetonitrile, chloroform, ethanol, methanol, and anhydrous dimethylformamide (DMF)), formic acid, and magnesium sulfate ($MgSO_4$) were purchased from Sigma-Aldrich. Pyridine (C_5H_5N) was purchased from Alfa Aesar. Phosphate buffer saline (PBS) was purchased from Fisher. Water used in all experiments was deionized to 18.2 MΩ (MILLIPORE). All chemicals were purchased at standard grades and used as received.

Methods. *Synthesis, Purification, and Characterization of 5-FCPal.* First, pyridine and 5′-DFCR were dissolved in

https://doi.org/10.1021/acs.molpharmaceut.1c00494
Mol. Pharmaceutics 2021, 18, 4331−4340

anhydrous DMF at the molar ratio of 5:1. Then, excess hexadecyl chloroformate (at a 2:1 molar ratio with 5′-DFCR) was added dropwise into the DMF mixture. The reaction was carried out overnight under nitrogen protection and constant stirring. Water was added into the reaction pot once it was finished, followed by adding chloroform to the mixture. The mixture was shaken well and placed still. Once phase separation occurred, the organic solvent was removed from the aqueous phase using a separatory funnel. The fresh chloroform solution was then added to the aqueous, and this step was repeated three times. Finally, all of the organic solution was pooled together, and $MgSO_4$ was added to absorb residual water that remained in the organic phase. $MgSO_4$ was filtered out, and the organic phase was transferred to the rotavap to evaporate all chloroform. The remaining solution formed a slight yellow and thick liquid. The liquid was then transferred to a flash column chromatography packed with silica. Ethyl acetate was used to separate the product (5-FCPal) from unreacted hexadecyl chloroformate. The reaction product was characterized using thin liquid chromatography (TLC), H^1 NMR, and high-performance liquid chromatography (HPLC) (Shimadzu, LC-20AP) (Figure S1).

HPLC Analysis. HPLC analysis was carried out on a Shimadzu HPLC system (Columbia, MD). Thermo Scientific Hypersil Gold C18 column (2.1 50 mm, 5 mm) was used for chromatographic separation. The mobile phase consists of a gradient method starting with 5% acetonitrile/95% 0.1% formic acid and reaching 95% acetonitrile/5% 0.1%formic acid in water over 7 min. The flow rate was set to be 1 mL/min. The injection volume to the column is 10 μL. The detection wavelength is 300 nm.

Surface Pressure−Mean Molecular Isotherm Measurements. A Langmuir trough with the dimension of 51 mm × 155 mm (KSV NIMA, Biolin Scientific) was used to measure surface pressure−mean molecular area isotherms of the monolayer on a PBS buffer. The temperature of the subphase was monitored by a thermocouple inserted in the subphase and controlled by a water circulation system (Anova Scientific) at 23 ± 0.5 °C. Interfacial tension was measured by a platinum Wilhelmy plate suspended from a wire that was attached to a film balance. All samples were dissolved in chloroform and stored at −20 °C. Before each measurement, the trough was cleaned thoroughly with chloroform, methanol, and deionized water and confirmed by a surface pressure fluctuation less than ±0.2 mN/m throughout the entire surface area change. The lipid was then spread dropwise at the interface using a syringe. To ensure complete solvent evaporation and the equilibrium of the monolayer, the system was left undisturbed for 15 min. The surface pressure−mean molecular area isotherm for the monolayer was recorded during compression by two symmetric barriers. Each one moved at 1.5 mm/min until the collapse of the monolayer.

Fluorescent Imaging of the Interface. For imaging, an epifluorescence microscope (Zeiss Observer, D1-AX10) was integrated with the Langmuir trough. 5-FCPal in chloroform with 1 μmol/mL concentration was mixed with 0.5 mol % of DPPE-Rhod to provide fluorescent contrast. The sample was spread on the PBS buffer within the Langmuir trough as described in the previous section. As the monolayer compressed, the solid domain formation was observed under the microscope. The incident light was provided by an X-Cite series 120 Q bulb with a TEXAS RED filter (Ex/Em 565/620 nm). The entire domain formation was recorded using AxioCam MRm camera (Zeiss) with a 20× air objective (LD-Plan-NEOFLUAR 20x).

X-ray Measurements. X-ray measurements were performed at the National Science Foundation's ChemMatCARS (15-IDC beamline) at the Advanced Photon Source (APS) user facility of the Argonne National Laboratory. The X-ray wavelength was 1.24 Å. Details of the experimental setup were described in our previous publications.[18−21] Briefly, a custom-made Langmuir trough (78 mm × 177.6 mm) with a single barrier was filled with 60 mL of PBS buffer. The trough is placed inside a gastight box. The interfacial tension was measured by using a paper Wilhelmy plate suspended from a balance (KSV Nima, Biolin Scientific). Before each measurement, the trough was cleaned thoroughly, the same as described in the previous session (2.2.3) of isotherm methodology. The samples were spread on top of the buffer, immediately followed by sealing the gastight box. Helium was used to purge the box until the oxygen level was below 2%. The monolayer was then compressed at a rate of 5 cm^2/min until the surface pressure reached 25 mN/m, at which the XR and GIXD measurements were carried out. The surface pressure was maintained at a constant 25 mN/m throughout the X-ray measurements by autoadjustment of the barrier position.

X-ray Data Analysis. The XR provides information on the packing structure normal to the air−liquid interface. The intensity of X-ray reflectivity (R) was measured at the different reflectivity angles corresponding to changes in the incident angles. The electron density profile was obtained after normalizing X-ray reflectivity (R) by the Fresnel reflectivity (R_F). The normalized X-ray reflectivity (R/R_F) data was fitted to a box model with electron density presented by a sum of error functions:[22]

$$\rho(z) = \frac{1}{2}\sum_{i=0}^{N} \mathrm{erf}\left(\frac{z - z_i}{\sqrt{2} \times \sigma}\right) \times (\rho_i - \rho_{i+1}) + \frac{\rho_0}{2}$$

where N is the number of slabs across the interface, z_i is the position of the i^{th} interface, σ is the roughness of the monolayer, ρ_i is the electron density of the i^{th} slab and ρ_0 is the electron density of the subphase.

GIXD is a function of horizontal wave vector Q_{xy} (parallel to the interface) and vertical wave vector Q_z (normal to the interface).[23,24] By varying both vectors, an area detector (Pilatus 200 K) was used to record the scattered X-ray intensity, which resulted in two-dimensional GIXD data. Bragg peaks and Bragg rods were obtained by integrating over the Q_z range and Q_{xy} range, respectively. By fitting the Bragg peaks using Gaussian functions and the out-plane Bragg rods using distorted wave Born approximation (DWBA),[25] information about the tilting angle and order of the molecules were obtained.

Formation of Prodrug-Loaded Liposomes. Thin-film dehydration method was used to prepare the prodrug-loaded liposomes with steps briefly as follows. All materials were dissolved in chloroform and kept at −20 °C. For generating nanoparticles of neutral lipids and the prodrug, 14.7 μL of 25 mg/mL DPPC with 31.4 μL of 50 mg/mL DOPC and 128.3 μL of 10 mg/mL 5-FCPal were pipetted into a 7 mL scintillation vial and dried under a gentle stream of Argon gas. The dried film was then placed under a vacuum for an additional 2 h to remove any residual traces of organic solvent. The desiccated film was subsequently rehydrated with 1 mL of

https://doi.org/10.1021/acs.molpharmaceut.1c00494
Mol. Pharmaceutics 2021, 18, 4331−4340

filtered, deionized H_2O (DI H_2O), and sonicated for approximately 5 min. Next, the nanoparticles of cationic lipids and the prodrug were prepared by mixing 14.1 μL of 25 mg/mL DSTAP with 27.9 μL of 50 mg/mL DOTAP and 128.3 μL of 10 mg/mL 5-FCPal. Subsequent procedure steps were the same as described for neutral lipids.

Measurements of Liposome Size and ζ Potential. The liposome sizes, reported as the intensity-weighted diameters, were characterized using dynamic light scattering (DLS) (Malvern Panalytical Zetasizer, Malvern, UK). Viscosity and refractive index of the solvent were set to be 1.0 cP and 1.333, respectively. The ζ potential was measured using Malvern Zetasizer.

RESULTS AND DISCUSSION

Interfacial Interaction of 5-FCPal with Positively Charged Lipids and Maximum Drug Loading. The interaction of the prodrug with the lipid molecules is mainly through the electrostatic type with the head groups and the hydrophobic type with the tail groups. Because of multiple functional groups of 5-FCPal, the charge distributions and interaction of the prodrug with the head groups of lipids are not obvious. Cationic lipids, which are usually included in the design of liposomes as transfection agents of DNAs and RNAs,[26] are first used to mix with 5-FCPal to evaluate the interaction between the prodrug and the lipid. A monolayer membrane of various molar fractions of 5-FCPal ($x_{5\text{-FCPal}}$ = 0.3, 0.5, 0.67, 0.77) with the saturated positively charged lipid, DSTAP (Figure 2A), was prepared at the gas–liquid interface

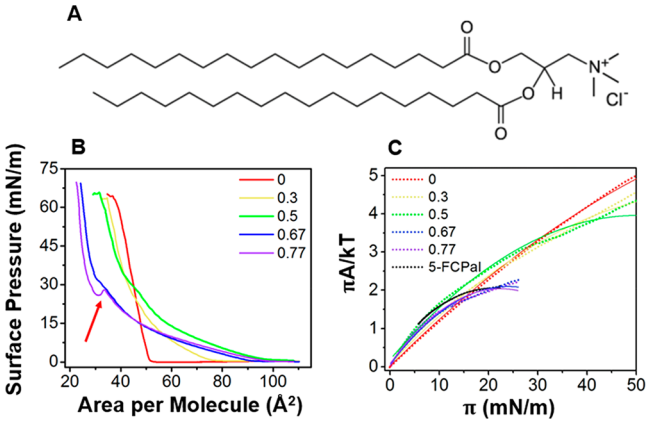

Figure 2. (A) Molecular structure of DSTAP. (B) Surface pressure–mean molecular area (π–A) curves of DSTAP and the mixtures of DSTAP and 5-FCPal at various ratios. The red arrow points to the transition phase that occurs once the mole fraction of the prodrug reaches 0.77. The legend indicates the molar fractions of the prodrug in the monolayer while the lipid concentration was kept at 1 μmol/mL. (C) Variation of $\pi A/kT$ values with a surface pressure at different mole fractions of 5-FCPal.

to quantify molecular packing of the mixtures. The surface pressure–mean molecular area (π–A) isotherms of the mixture of DSTAP and 5-FCPal are presented in Figure 2B. Under lateral compression, the isotherm of DSTAP has a rapid transition from liquid expanded (LE) phase to condensed (C) phase with LE-LC transition phase nearly undetectable.[27,28] The molecular packing of the saturated cationic lipid, DSTAP, is very close to a rigid solid monolayer, which explains that the saturated lipids are not able to form vesicles without combining with the unsaturated lipids. Adding 5-FCPal significantly affects the molecular packing of DSTAP. The slopes of the increasing surface pressure displayed the LE-C transition phase between LE and C phases. Although below 15 mN/m, adding 5-FCPal increased the mean molecular area above 30 mN/m, adding the prodrug makes the molecular packing even tighter.

Figure 2C shows a plot of $\pi A/kT$ versus π, which indicated the nonideal surface pressure, area, and temperature behavior of the DSTAP and the mixture of DSTAP and the prodrug monolayers. The data were fitted using the two-dimensional virial equation of state as,

$$\frac{\pi A}{kT} = b_0 + b_1\pi + b_2\pi^2$$

where b_0, b_1, and b_2 are the virial coefficients. The value of b_0 provides information about the aggregation state of the molecules, as π tends toward zero. The value of b_1 is attributed to the exclusion volumes and the interaction between the molecules, with negative and positive values indicting attraction and repulsion, respectively. The virial coefficients obtained from the fitting are listed in Table S1. The values of b_2 in this study are insignificant. For DSTAP monolayer film, the positive value of the second virial coefficient, b_1, indicates that electrostatic repulsion of the head groups is predominant. Adding 5-FCPal results in a small increase of b_1, denoting a slightly bigger repulsion between the molecules, which may be caused by simultaneously affecting both head and tail group interactions. With the mole fraction of 5-FCPal reaching more than 50%, the obtained virial coefficients have limited variation, approaching the second virial coefficient value of the pure prodrug monolayer.

To further quantify the lateral packing structure of the molecules, synchrotron X-ray surface scattering techniques, gracing-incident X-ray diffraction (GIXD), and X-ray reflectivity (XR) were employed. The Bragg peak positions of the out-plane peak shifted from 1.366 to 1.427 Å^{-1}, and the in-plane peak shifted from 1.462 to 1.482 Å^{-1} (Figure 3A). The shift of the GIXD peaks confirmed that the molecular packing at the constant consistent pressure is tighter when adding more 5-FCPal. GIXD rods shifted toward lower Q_z (Figure S2), indicating a decrease in the tilt angles of the molecules (from 32.5° to 24.8°) (Table S5). The intensity of the Bragg peaks decreases with more 5-FCPal added to the membrane, indicating the decrease in surface coverage of lipid domains.

Using the box model, XR data were fitted to obtain the electron density (Figure 3B,C) of the monolayer. The fitting parameter and the structural parameters are listed in Table S6. At 25 mN/m, the DSTAP monolayer has a total thickness of 24.6 Å. Adding 5-FCPal at $x_{5\text{-FCPal}}$ = 0.3, the thickness of the headgroup increases from 6.6 to 15.5 Å. As the mole fraction of the prodrug increases, the headgroup region becomes thicker, while the hydrocarbon tail region thickness remains similar. However, as the prodrug mole fraction reached 0.77, there was little change to the XR results. The isotherm and X-ray results suggest that the maximum mole fraction of 5-FCPal in the liposomes should not exceed 0.67.

Another observation from the π–A isotherm is that once the mole fraction of the prodrug exceeds 0.67, surface pressure no longer monotonically increases when the surface is compressed, and the isotherm exhibits a small transition phase at the surface pressure of about 28 mN/m. With $x_{5\text{-FCPal}}$ = 0.77, it is obvious that when the membrane was continuously

https://doi.org/10.1021/acs.molpharmaceut.1c00494
Mol. Pharmaceutics 2021, 18, 4331–4340

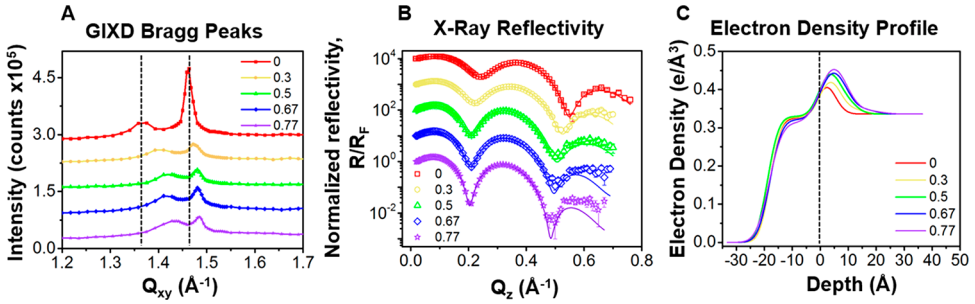

Figure 3. (A) GIXD Bragg peaks of DSTAP and 5-FCPal mixtures. Data was offset for clarity. The dash lines indicate the peak position of the in-plane Bragg peak of the DSTAP monolayer. (B) Normalized XR data of DSTAP and 5-FCPal mixtures on the PBS subphase. The solid lines show the best fit of the data using the box model. The data were offset for clarity. (C) Corresponding electron density profile for DSTAP and 5-FCPal mixtures. The dashed line (z = 0) was artificially decided to be the water−air interface.

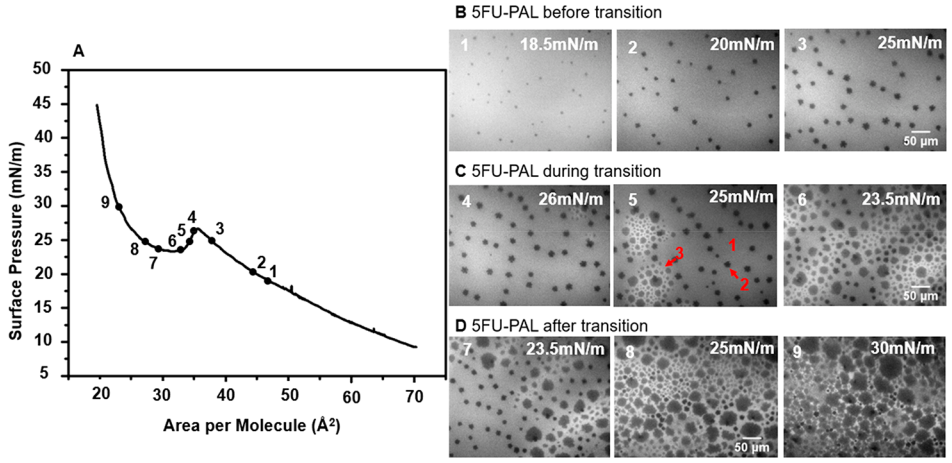

Figure 4. (A) 5-FCPal isotherm. The numbers on the isotherm correspond to the fluorescent images in B−D taken at the specific surface pressure. (B) Evolution sequences of 5-FCPal domain formation of the monolayer membrane. The solid domains formed at the interface are shown as dark gray spots. (C) Evolution sequences of 5-FCPal domains change from monolayer to multilayer structure during the transition. The red arrows indicate the monolayer and multilayer domains formed at the interface. Number 1 in the gray area indicates the monolayer liquid domain. Number 2 and the arrow pointing to a dark spot indicate the monolayer solid domain. Number 3 and the arrow pointing to a bright area indicate the multilayer domain. (D) Fluorescent images of the membrane with multilayer domains continuing to expand after the transition.

compressed, the surface pressure first dropped and then increased (indicated by the red arrow in Figure 2B). The drop of the pressure indicated the collapse of the monolayer membrane or the formation of domains with multilayer structures. Because the film is highly ordered and closely packed, it is able to continue to increase the surface pressure until the film collapse at a similar pressure as the DSTAP film.

To investigate the transition seen in the isotherm in Figure 2B, a pure 5-FCPal monolayer was spread onto PBS buffer, and a fluorescent microscope was integrated to capture images in real-time as the layer compressed. Figure 4A shows a transition phase in the 5-FCPal isotherm where the surface pressure decreases slightly from 27 to 23 mN/m and then increases again from 23 mN/m with a steeper slope. Fluorescent images show that the solid domain formation of 5-FCPal starts at 18 mN/m and slowly expands as the surface pressure increases but still maintains its monolayer integrity (Figure 4B). However, further compression caused the formation of the multilayer domains, indicated in the fluorescent images (Figure 4C) by different fluorescent intensities (bright gray and dark gray marked with red arrows). After the transition, the multilayer domains become dominant, and they continue to expand as the surface pressure continues to increase (Figure 4D). Furthermore, the compression and expansion isotherm loop exhibit hysteresis (Figure S3), with significant deviation observed when comparing the expansion trace to the monolayer region (before the transition) of the compression isotherm. The expansion isotherm shifts to a smaller area per molecule, and it cannot reach the same starting area per molecule as the compression curve (45 Å^2 and 55 Å^2, respectively), suggesting that the highly ordered multilayer domains are irreversible once formed.

The electron density profile of the film of 5-FCPal before multilayer formation shows that under lateral compression, the prodrug head groups were protruded into the aqueous subphase. This causes the packing to become tighter. Therefore, the thickness of the headgroup region is significantly increased (from 11.5 Å at 10 mN/m to 20.3 Å at 18.5 mN/m) (Figure S4 and Table S7). The tail length only increased slightly, but the electron density of the tail groups went from 0.28 to 0.33 (eÅ^{-3}) (Table S7). This suggests that due to the protrusion of the headgroup into the subphase, the hydrophobic tails are being packed tight together, which causes the solid domains to form. Based on GIXD data, the prodrug packing structure is hexagonal, and the increase in the intensity of the Bragg peak shows that the surface coverage of the solid domain increases as the surface pressure increases. After the transition, the monolayer box model is no longer suitable to fit

https://doi.org/10.1021/acs.molpharmaceut.1c00494
Mol. Pharmaceutics 2021, 18, 4331−4340

the data as the surface becomes incredibly rough and heterogeneous. These data suggest that the multiplayer formation of the 5-FCPal domain would cause instability of the molecular packing, which should be avoided when designing stable liposomes or nanoparticles. Therefore, a theoretical maximum drug loading of the liposomes could be set as the amount of the prodrug in the film before the formation of the complex multilayer structure.

To further examine the effect of adding 5-FCPal to the monolayer of lipids, a similar cationic lipid with unsaturated tail groups, DOTAP (Figure 5A), was used for the same measurements. Because of the unsaturation, the hydrophobic interaction of the DOTAP tail groups is greatly reduced, compared to DSTAP. The influence of adding 5-FCPal to the lipid monolayer would be mainly through interrupting the electrostatic interaction of the lipid head groups. The surface pressure isotherm continuously shifted to the smaller molecular area in the presence of more of the prodrug (Figure 5B), denoting that the packing of the molecules at the interface becomes tighter. This is also confirmed by obtaining the values of the virial coefficients. With more 5-FCPal added to the monolayer film, the second virial coefficient, b_1, keeps reducing to a smaller positive value, indicating less repulsion from the molecules (Figure 5C and Table S2).

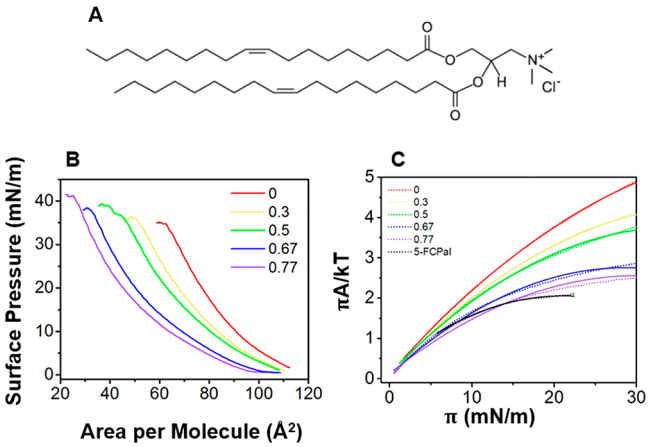

Figure 5. (A) Molecular structure of DOTAP. (B) Surface pressure−mean molecular area (π−A) curves of DOTAP and the mixtures of DOTAP and 5-FCPal at various ratios. The legend indicates the molar fractions of the prodrug in the monolayer while the lipid concentration was kept at 1 μmol/mL. (C) Variation of $\pi A/kT$ values with a surface pressure at different mole fractions of 5-FCPal.

DOTAP molecules are incapable of forming ordered structures due to their unsaturation. Therefore, it is expected that no Bragg peak was observed by GIXD. However, once the prodrug molar fraction reached 0.77, a single in-plane Bragg peak at about 1.5 $Å^{-1}$ was detected, which was from the hexagonal packing of the hydrocarbon tails of the 5-FCPal molecules (Figure 6A). The Bragg rod (Q_z = 0) indicates the zero-tilt angle of the molecules. The GIXD data in Figure 6B suggests that as the mole fraction of the prodrug reaches 0.77, domain separation between the lipid and the prodrug is significant. XR reveals strong interaction between the headgroup of the lipid and the polar part of the prodrug (Figure 6C). Specifically, the monolayer of DOTAP has a total thickness of 17.3 Å (Table S8). Adding 5-FCPal to the monolayer shifted the peak of XR to a lower Q_z, increased the thickness of the headgroup region to 12.7 Å, and kept the thickness of the hydrocarbon tail around 12 Å. Once the mole fraction of the 5-FCPal reaches 0.77, the XR curve is significantly changed, and the fitting suggests that a layer of 10 Å is underneath the typical monolayer headgroup region. This is consistent with the size of the 5-FCPal polar part (Table S7).

From the results, the cationic lipids would be potentially able to form stable vesicles with 5-FCPal. However, a combination of saturated and unsaturated lipids to balance the rigidity and flexibility of lipid vesicles is necessary for the design of stable and high drug-loading liposomes. The formation of the highly ordered domain of the prodrug limits the drug loading not exceeding 67 mol %.

Interfacial Interaction of 5-FCPal with Neutral and Negatively Charged Lipids. To examine the effects of the headgroup charges on the interaction of the lipids with the prodrug, the interfacial molecular packing of DPPC (with the zwitterionic headgroup) (Figure 7A) and DPPG (with the negatively charged headgroup) (Figure 9A) with various amount of the prodrug was explored. The saturated lipids were chosen for obtaining more molecular packing information from GIXD. Adding 5-FCPal to DPPC or DPPG, the isotherms present significant changes (Figures 7B and 9B). Upon fitting the variation of $\pi A/kT$ with surface pressure for both DPPC and DPPG (Figures 7C and 9C), with 30% of 5-FCPal, b_1 is promptly increased to the value similar to the film of the prodrug, representing a larger increase in repulsion

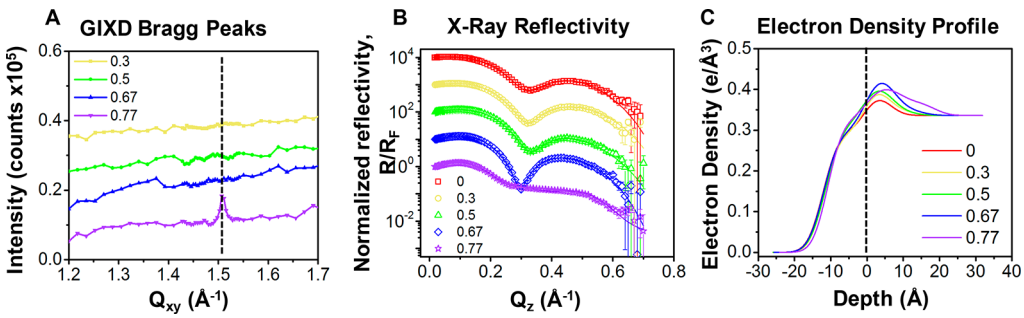

Figure 6. (A) GIXD Bragg peaks of DOTAP and 5-FCPal mixtures. Data was offset for clarity. The dash lines indicate the peak position of the in-plane Bragg peak. (B) Normalized XR data of DOTAP and 5-FCPal mixtures on the PBS subphase. The solid lines show the best fit of the data using the box model. The data was offset for clarity. (C) Corresponding electron density profile for DOTAP and 5-FCPal mixtures. The dashed line (z = 0) was artificially decided to be the water−air interface.

https://doi.org/10.1021/acs.molpharmaceut.1c00494
Mol. Pharmaceutics 2021, 18, 4331−4340

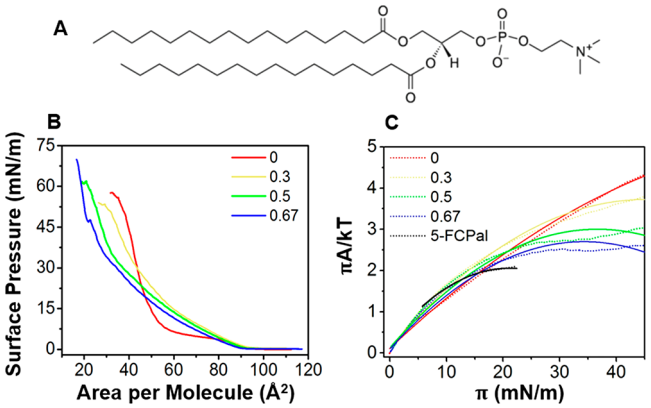

Figure 7. (A) Molecular structure of DPPC. (B) Surface pressure−mean molecular area (π−A) curves of DPPC and the mixtures of DPPC and 5-FCPal at various ratios. The legend indicates the molar fractions of the prodrug in the monolayer while the lipid concentration was kept at 1 μmol/mL. (C) Variation of $\pi A/kT$ values with a surface pressure at different mole fractions of 5-FCPal.

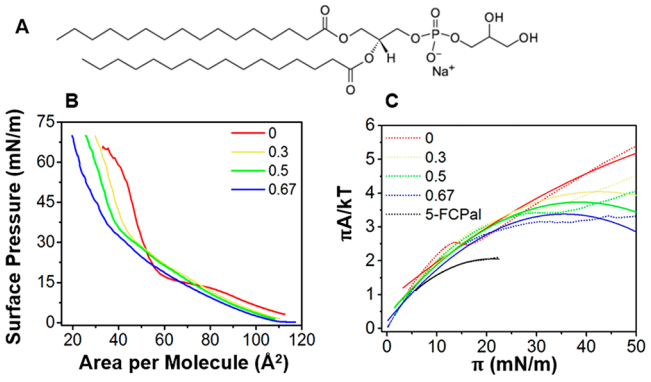

Figure 9. (A) Molecular structure of DPPG. (B) Surface pressure−mean molecular area (π−A) curves of DPPG and the mixtures of DPPG and 5-FCPal at various ratios. The legend indicates the molar fractions of the prodrug in the monolayer while the lipid concentration was kept at 1 μmol/mL. (C) Variation of $\pi A/kT$ values with a surface pressure at different mole fractions of 5-FCPal.

between molecules, compared to the monolayer film of DSTAP mixed with the prodrug (Tables S3 and S4).

GIXD and XR were used to provide more detailed information about the interaction between the molecules. For DPPC, both out-of-plane and in-plane Bragg peaks shift slightly to higher Q_{xy}, which indicates slightly tighter packing of the tail groups (Figure 8A). The calculated molecular area was decreased from 48.6 Å^2 to 46 Å^2. The tilt angle of the lipid molecules also decreases from 33.3° to 27° (Table S9). Although GIXD suggests that 5-FCPal caused the packing of DPPC to be tighter, the effect is not as significant as seen with DSTAP. By fitting the XR data (Figure 8B), it is revealed that with a 0.33 molar fraction of the prodrug added to the monolayer, the electron density of the headgroup remains the same, and the thickness of the headgroup region increases from 8.6 to 20 Å. The hydrocarbon tail thickness decreases from 16.5 to12 Å (Figure 8C and Table S10) due to the short tail length of the prodrug (Table S7). As the mole fraction of 5-FCPal increases, the effect remains similar. The X-ray data suggest that the headgroup interaction between 5-FCPal and DPPC is weaker than in the case of DSTAP; therefore, despite the prodrug causing the packing of the lipid molecules to be slightly tighter, the overall thickness of the tail group decreased.

For anionic lipid DPPG, the Bragg peak positions of the in-plane and the out-of-plane peaks remain the same at 1.46 and 1.35 Å^{-1}, respectively, even with 5-FCPal added to the monolayer (Figure 10A). Since the GIXD peaks are from the carbon tails of the lipid, the peak intensities decreased once the prodrug was added. There is very little change for the tilt angle from 32.2° to 31.5°(Table S11). XR result (Figure 10B) shows that the DPPG monolayer has a total thickness of 26 Å, which is consistent with the values reported in previous studies.[29] With the addition of 5-FCPal, the thickness of the headgroup increases from 8.7 to 20 Å (Table S12), and the hydrocarbon tail thickness decreases from 17 to12 Å. Furthermore, Figure 10C shows a decrease in headgroup electron density when adding 5-FCPal. The XR data suggests that the 5-FCPal did not interact with DPPG in the headgroup region, and it is possible that the prodrug molecules stay outside of the lipid domains, which caused the electron density of the headgroup to drop.[29]

Design of 5-FCPal Nanoformulation. Based on the information provided by the X-ray surface measurements, it is predicted that the liposome formed by the combination of saturated and unsaturated cationic lipids and 5-FCPal with drug loading less than 66% would be most stable. As a comparison, nanoparticles of cationic lipids and 5-FCPal, neutral lipids with 5-FCPal, and pure prodrug were generated by the film-rehydration process. Although 5-FCPal is an

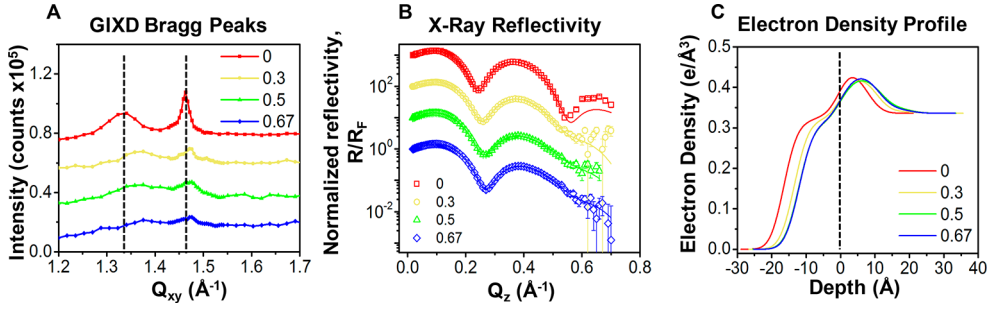

Figure 8. (A) GIXD Bragg peaks of DPPC and 5-FCPal mixtures. Data was offset for clarity. The dash lines indicate the DPPC peak position of the in-plane Bragg peak. (B) Normalized XR data of DPPC and 5-FCPal mixtures on the PBS subphase. The solid lines show the best fit of the data using the box model. The data was offset for clarity. (C) Corresponding electron density profile for DPPC and 5-FCPal mixtures. The dashed line (z = 0) was artificially decided to be the water−air interface.

https://doi.org/10.1021/acs.molpharmaceut.1c00494
Mol. Pharmaceutics 2021, 18, 4331−4340

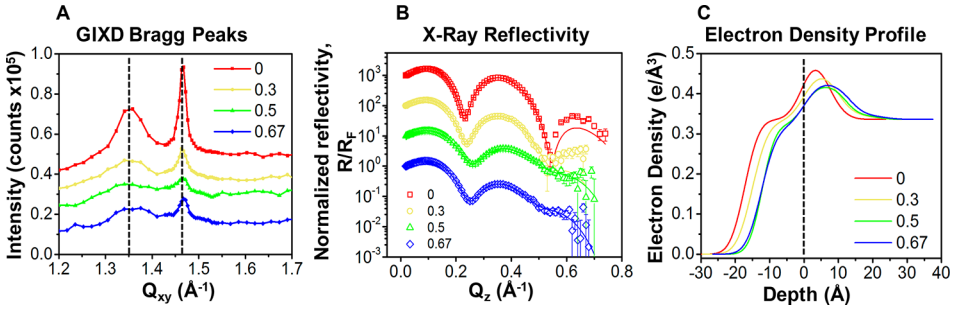

Figure 10. (A) GIXD Bragg peaks of DPPG and 5-FCPal mixtures. Data was offset for clarity. The dash lines indicate the DPPG peak position of the in-plane Bragg peak. (B) Normalized XR data of the DPPG and 5-FCPal mixtures on the PBS subphase. The solid lines show the best fit of the data using the box model. The data was offset for clarity. (C) Corresponding electron density profile for DPPG and 5-FCPal mixtures. The dashed line (z = 0) was artificially decided to be the water−air interface.

amphiphilic molecule, at the interface, a multilayer structure is formed because of the bulky charged headgroup and the single hydrophobic tail of the molecule (Figure 4). Therefore, the pure prodrug would form bigger aggregates instead of submicrometer liposomes or nanoparticles (Figure 11A).

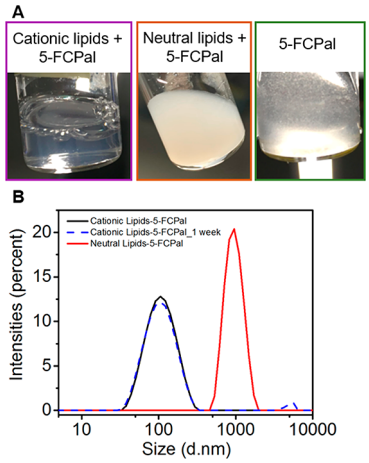

Figure 11. (A) Images of particle suspensions generated using the film dehydration method. Left: the mixture of cationic lipids with 5-FCPal. The molar ratio is DSTAP/DOTAP/5-FCPal 1:4:5. Middle: the mixture of neutral lipids with 5-FCPal. The molar is DPPC/DOPC/5-FCPal 1:4:5. Right: pure 5-FCPal suspension. (B) DLS measurements of the particle size distribution for the suspensions containing the prodrug and the cationic lipids (DSTAP/DOTAP/5-FCPal 1:4:5) (black solid curve) and the neutral lipids (DPPC/DOPC/5-FCPal 1:4:5) (red solid curve). The size of the nanoparticle suspension of the cationic lipids and 5-FCPal was measured a week after, showing one-week stability of the nanoparticle suspension (blue dash curve).

With neutral lipids mixed with the prodrug, the average size of the particles is about 1000 nm. With cationic lipids mixed with prodrug, the average size of the liposome is about 100 nm with a narrow size distribution, with a single peak at about 100 nm, which is feasible for IV injection, long-term blood circulation, and the possibility of taking advantage of EPR effect for passive drug accumulation at the tumor sites (Figure 11B). However, positive lipids are considered toxic because they would introduce significant disturbance to the cell membrane. Therefore, the surface charges of the particles need to be shielded for biomedical applications. By adding 5% molar of PEGylated lipid DPPE-PEG5k, which has a limited effect on lipid molecular packing and interaction,[18] the surface charge of the nanoparticles reduced to 4.14 ± 0.9 mV (which is considered neutral) from 30.6 ± 4.4 mV without the PEGylated lipid (Figure 12B), while the size remained at 90.4 ± 1.4 nm (Figure 12A).

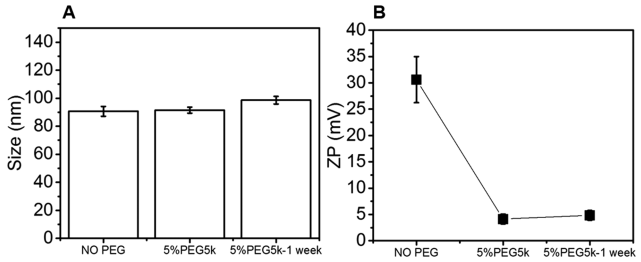

Figure 12. Neutralization of the surface charges of the nanoparticles comprising cationic lipids and 5-FCPal liposomes by adding 5% mol of DPPE-PEG5k. (A) Nanoparticle size and (B) ζ potential before and after adding DPPE-PEG5k.

CONCLUSIONS

The information obtained from interfacial isotherm and synchrotron X-ray surface scattering measurements provides insights into the drug interaction with different lipids and helps design an effective liposome formulation with high drug loading. At the same surface pressure, mixing the amphiphilic prodrug with the cationic lipids caused the monolayer packing of the molecules to be tighter. However, little effect on molecular packing structure has been detected by GIXD for the mixture of the prodrug with the neutral and anionic lipids. The GIXD measurements also indicate that when the content of the prodrug at the interface reaches 67 mol %, the prodrug domains may form multilayer structures. Liposomal formulation of the mixture of saturated and unsaturated cationic lipids with 50 mol % (or 43 wt %) drug loading of 5-FCPal was generated and characterized to demonstrate that the XR and GIXD measurements give a reliable indication for the design of the nanoparticle formulation. Because the interaction of the 5-FU prodrug is mainly through the electrostatic interaction with the head groups, the results may be applied for other analogues of 5-FCPal, including capecitabine. Employing the interfacial techniques, the number of trials may be significantly reduced in choosing lipids as nanocarriers for amphiphilic prodrugs through a fundamental understanding of molecular interaction at the interface.

https://doi.org/10.1021/acs.molpharmaceut.1c00494
Mol. Pharmaceutics 2021, 18, 4331−4340

■ ASSOCIATED CONTENT

Supporting Information

The Supporting Information is available free of charge at https://pubs.acs.org/doi/10.1021/acs.molpharmaceut.1c00494.

Additional data analysis and characterization (PDF)

■ AUTHOR INFORMATION

Corresponding Author

Ying Liu − *Department of Chemical Engineering, University of Illinois at Chicago, Chicago, Illinois 60608, United States; Department of Bioengineering and Department of Biopharmaceutical Sciences, University of Illinois at Chicago, Chicago, Illinois 60607, United States;* orcid.org/0000-0002-1207-8409; Email: liuying@uic.edu

Authors

Tiep Pham − *Department of Chemical Engineering, University of Illinois at Chicago, Chicago, Illinois 60608, United States*

Paola Leon Plata − *Department of Chemical Engineering, University of Illinois at Chicago, Chicago, Illinois 60608, United States*

Pin Zhang − *Department of Chemical Engineering, University of Illinois at Chicago, Chicago, Illinois 60608, United States;* orcid.org/0000-0003-0107-221X

Anand Vellara − *Department of Chemical Engineering, University of Illinois at Chicago, Chicago, Illinois 60608, United States*

Wei Bu − *NSF's ChemMatCARS and Pritzker School of Molecular Engineering, University of Chicago, Chicago, Illinois 60637, United States;* orcid.org/0000-0002-9996-3733

Binhua Lin − *NSF's ChemMatCARS and Pritzker School of Molecular Engineering, University of Chicago, Chicago, Illinois 60637, United States;* orcid.org/0000-0001-5932-4905

Gang Cheng − *Department of Chemical Engineering, University of Illinois at Chicago, Chicago, Illinois 60608, United States;* orcid.org/0000-0002-7170-8968

Complete contact information is available at: https://pubs.acs.org/10.1021/acs.molpharmaceut.1c00494

Notes

The authors declare no competing financial interest.

■ ACKNOWLEDGMENTS

The study is partially supported by the gift fund by CurMed Pharmaceuticals INC. NSF's ChemMatCARS Sector 15 is supported by the Divisions of Chemistry (CHE) and Materials Research (DMR), National Science Foundation, under grant no. NSF/CHE-1834750. Use of the Advanced Photon Source, an Office of Science User Facility operated for the U.S. Department of Energy (DOE) Office of Science by Argonne National Laboratory, was supported by the U.S. DOE under contract no. DE-AC02-06CH11357.

■ REFERENCES

(1) Pang, A. High-loading Gα13-binding EXE peptide nanoparticles prevent thrombosis and protect mice from cardiac ischemia/reperfusion injury. *Sci. Transl. Med.* **2020**, *12* (552), 1.

(2) Tang, Q.; Cao, B.; Wu, H.; Cheng, G. Cholesterol-Peptide Hybrids to Form Liposome-Like Vesicles for Gene Delivery. *PLoS One* **2013**, *8* (1), e54460.

(3) Tang, Q.; Cao, B.; Cheng, G. Co-delivery of small interfering RNA using a camptothecin prodrug as the carrier. *Chem. Commun.* **2014**, *50* (11), 1323−1325.

(4) Ma, W.; et al. Synergistic antitumor activity of a self-assembling camptothecin and capecitabine hybrid prodrug for improved efficacy. *J. Controlled Release* **2017**, *263*, 102−111.

(5) Barenholz, Y. Doxil(R)–the first FDA-approved nano-drug: lessons learned. *J. Controlled Release* **2012**, *160* (2), 117−34.

(6) O'Brien, M. E.; et al. Reduced cardiotoxicity and comparable efficacy in a phase III trial of pegylated liposomal doxorubicin HCl (CAELYX/Doxil) versus conventional doxorubicin for first-line treatment of metastatic breast cancer. *Ann. Oncol* **2004**, *15* (3), 440−9.

(7) Safra, T.; et al. Pegylated liposomal doxorubicin (doxil): reduced clinical cardiotoxicity in patients reaching or exceeding cumulative doses of 500 mg/m2. *Ann. Oncol* **2000**, *11* (8), 1029−33.

(8) Khurana, A.; et al. Role of nanotechnology behind the success of mRNA vaccines for COVID-19. *Nano Today* **2021**, *38*, 101142.

(9) Park, K. S.; et al. Non-viral COVID-19 vaccine delivery systems. *Adv. Drug Delivery Rev.* **2021**, *169*, 137−151.

(10) Twelves, C.; et al. Capecitabine as adjuvant treatment for stage III colon cancer. *N. Engl. J. Med.* **2005**, *352* (26), 2696−2704.

(11) Wagstaff, A. J.; Ibbotson, T.; Goa, K. L. Capecitabine: a review of its pharmacology and therapeutic efficacy in the management of advanced breast cancer. *Drugs* **2003**, *63* (2), 217−36.

(12) Aguirre-Chagala, Y. E.; et al. Phenylboronic Acid-Installed Polycarbonates for the pH-Dependent Release of Diol-Containing Molecules. *ACS Macro Lett.* **2014**, *3* (12), 1249−1253.

(13) Gong, X.; et al. Lamellar crystalline self-assembly behaviour and solid lipid nanoparticles of a palmityl prodrug analogue of Capecitabine–a chemotherapy agent. *Colloids Surf., B* **2011**, *85* (2), 349−59.

(14) Reigner, B.; Blesch, K.; Weidekamm, E. Clinical pharmacokinetics of capecitabine. *Clin. Pharmacokinet.* **2001**, *40* (2), 85−104.

(15) Miwa, M.; et al. Design of a novel oral fluoropyrimidine carbamate, capecitabine, which generates 5-fluorouracil selectively in tumours by enzymes concentrated in human liver and cancer tissue. *Eur. J. Cancer* **1998**, *34* (8), 1274−1281.

(16) Sagnella, S. M.; et al. Nanostructured nanoparticles of self-assembled lipid pro-drugs as a route to improved chemotherapeutic agents. *Nanoscale* **2011**, *3* (3), 919−924.

(17) Aranda, J.; et al. The catalytic mechanism of carboxylesterases: a computational study. *Biochemistry* **2014**, *53* (36), 5820−9.

(18) Zhang, P.; et al. Impeded Molecular Reorganization by Polyethylene Glycol Conjugation Revealed by X-ray Reflectivity and Diffraction Measurements. *Langmuir* **2020**, *36* (26), 7573−7581.

(19) Zhang, P.; et al. Spontaneous collapse of palmitic acid films on an alkaline buffer containing calcium ions. *Colloids Surf., B* **2020**, *193*, 111100.

(20) Zhang, P.; et al. Molecular interactions of phospholipid monolayers with a model phospholipase. *Soft Matter* **2019**, *15* (20), 4068−4077.

(21) Zhang, P.; et al. Polyunsaturated Phospholipid Modified Membrane Degradation Catalyzed by a Secreted Phospholipase A2. *Langmuir* **2019**, *35* (36), 11643−11650.

(22) Parratt, L. G. Surface Studies of Solids by Total Reflection of X-Rays. *Phys. Rev.* **1954**, *95* (2), 359−369.

(23) Kjaer, K.; et al. Ordering in lipid monolayers studied by synchrotron x-ray diffraction and fluorescence microscopy. *Phys. Rev. Lett.* **1987**, *58* (21), 2224−2227.

(24) Dutta, P.; et al. X-ray diffraction studies of organic monolayers on the surface of water. *Phys. Rev. Lett.* **1987**, *58* (21), 2228−2231.

(25) Bu, W.; Vaknin, D. Bilayer and trilayer crystalline formation by collapsing behenic acid monolayers at gas/aqueous interfaces. *Langmuir* **2008**, *24* (2), 441−447.

(26) Lu, J. J.; Langer, R.; Chen, J. A novel mechanism is involved in cationic lipid-mediated functional siRNA delivery. *Mol. Pharmaceutics* **2009**, *6* (3), 763−771.
(27) Moghaddam, B.; et al. Exploring the correlation between lipid packaging in lipoplexes and their transfection efficacy. *Pharmaceutics* **2011**, *3* (4), 848−864.
(28) Christensen, D.; et al. alpha, alpha'-trehalose 6,6′-dibehenate in non-phospholipid-based liposomes enables direct interaction with trehalose, offering stability during freeze-drying. *Biochim. Biophys. Acta, Biomembr.* **2008**, *1778* (5), 1365−73.
(29) Andreev, K.; et al. Hydrophobic interactions modulate antimicrobial peptoid selectivity towards anionic lipid membranes. *Biochim. Biophys. Acta, Biomembr.* **2018**, *1860* (6), 1414−1423.

https://doi.org/10.1021/acs.molpharmaceut.1c00494
Mol. Pharmaceutics 2021, 18, 4331−4340